Biosensors and Bioelectronics 26 (2011) 4088–4094

Contents lists available at ScienceDirect

Biosensors and Bioelectronics

journal homepage: www.elsevier.com/locate/bios

A biocompatible titanium nitride nanorods derived nanostructured electrode for biosensing and bioelectrochemical energy conversion

Shanmu Dong[a,1], Xiao Chen[a,1], Lin Gu[b], Lixue Zhang[a], Xinhong Zhou[c], Zhihong Liu[a], Pengxian Han[a], Hongxia Xu[a], Jianhua Yao[a], Xiaoying Zhang[a], Lanfeng Li[c], Chaoqun Shang[c], Guanglei Cui[a,*]

[a] Key Laboratory of Biofuels, Qingdao Institute of Bioenergy and Bioprocess Technology, Chinese Academy of Sciences, Qingdao 266101, PR China
[b] WPI Advanced Institute for Materials Research, Tohoku University, Sendai 9808577, Japan
[c] Qingdao University of Science and Technology, Qingdao 266101, PR China

ARTICLE INFO

Article history:
Received 10 January 2011
Received in revised form 30 March 2011
Accepted 30 March 2011
Available online 7 April 2011

Keywords:
Titanium nitride
Nanorod arrays
Nanostructured electrodes
Bio-Li–air fuel cell

ABSTRACT

In this study, a facile method is proposed to fabricate biocompatible TiN nanorod arrays through solvent-thermal synthesis and subsequent nitridation in ammonia atmosphere. The TiN nanorod arrays are potential excellent nanostructured electrodes owing to their good electronic conductivity and large surface area. These nanostructured electrodes not only deliver superior electrocatalytic activity (the limit of detection, LOD is 0.5 μM) and highly selective sensing towards H_2O_2, but also exhibit excellent biocompatibility with horseradish peroxidase (HRP) in a highly sensitive enzymatic biosensor for H_2O_2 (the LOD can reach to 0.05 μM). Furthermore, a novel biocatalytic cathode based Li air fuel cell (bio-Li–air fuel cell) is explored based on the combination of TiN nanorod arrays and laccase (LAC) for electrochemical energy conversion. These results demonstrate that TiN nanorod arrays can be served as excellent nanostructured electrodes for multifunctional bioelectrochemical applications.

1. Introduction

Nanostructured electrodes can be potentially used in the areas of online real-time analysis, sensitive detection and in vivo power sources (Njagi et al., 2010; Swensen et al., 2009; Wang et al., 2008; Yan et al., 2009; Zelada-Guillén et al., 2009; Zhou et al., 2010). For these applications, these electrodes need to meet some important criteria including: (1) large surface-to-bulk ratio, (2) high electrochemical activity, and (3) good biocompatibility (Zayats et al., 2008; Zhang et al., 2009; Zhou et al., 2008). In recent years, nanorod or nanotube arrays growing directly on a current collector have been intensively investigated to prepare nanostructured electrodes for biosensor and biofuel cell application, as their well defined one-dimensionality (1D) structure is favorable for accessible diffusion of ions and electron mediators and ensures a beneficial connection between electroactive materials and substrate (Kafi et al., 2008; Xiao et al., 2007; Yang et al., 2009; Zhang et al., 2009). On the other hand, TiN has drawn considerable attention for their wide application in a variety of applications (Drygas et al., 2006; Qiu and Gao, 2005). Because of its superior hardness, corrosion resistance, high melting point and low electronic resistivity, TiN was reported to serve as abrasives and protective coating, electrodes for supercapacitors (Choi and Kumta, 2006), catalyst (Fischer et al., 2008; Kaskel et al., 2004; Muhammed Musthafa and Sampath, 2008; Yao et al., 2009) and also a promising conductive additive for lithium-ion batteries (Qiu and Gao, 2005; Snyder et al., 2007). Recent reports have also found its potential use as electrodes for chemical sensing (Kirchner et al., 2007; Wang et al., 2006). Although TiN has always been viewed as an excellent biocompatible material for coating in biomedical application (Hyde et al., 2009; Serro et al., 2009), to the best of our knowledge, there is still limited reports of TiN in bioelectrochemical application, such as biosensor or other bioelectrochemical energy conversion systems. Therefore, TiN nanorod arrays can be expected to possess good conductivity and biocompatibility with unique 1D nanostructure, which are desirable for the electrodes of bioelectrochemical sensing and energy conversion systems.

In the present work, we report a facile method preparing TiN nanorod arrays (TiN NRAs) directly grown on Ti foil substrate by solvent-thermal synthesis and subsequent nitridation using ammonia annealing. Based on TiN NRAs, a nanostructed electrode was developed. It can be used as the electrodes for electrochemical sensing and biosensing towards hydrogen peroxide (H_2O_2). In addition, although substantial researches have employed kinds of enzymes (Deng et al., 2008; Noh et al., 2010; Tasca et al., 2008; Yan et al., 2009) and hemoproteins (Katz et al., 2005; Ramanavicius and Ramanaviciene, 2009) to fabricate enzymatic electrode for biofuel

* Corresponding author. Tel.: +86 532 80662746; fax: +86 532 80662744.
E-mail addresses: dongsm@qibebt.ac.cn (S. Dong), cuigl@qibebt.ac.cn (G. Cui).
[1] These authors contributed equally to this work.

0956-5663/$ – see front matter © 2011 Elsevier B.V. All rights reserved.
doi:10.1016/j.bios.2011.03.040

cell, there is still no report concerning involving enzymatic cathode into Li air batteries. Therefore, a novel energy conversion system of "bio-Li–air fuel cell" was also explored in this study using the TiN NRAs as a supporter of enzymatic air-electrode. It is demonstrated that TiN NRAs showing promising electrochemical performance should be extremely attractive for a wide range of electrochemical sensing, biosensing, and bioeletctrochemical energy conversion applications.

2. Experimental

2.1. Preparation of TiN NRAs

All chemicals were used as received without further purification. TiO_2 nanorod arrays were synthesized as a similar recipe described in the literature (Feng et al., 2008). In a typical synthesis, 10 mL of toluene was mixed with 1 mL titanium tetrachloride (1 M) in toluene (97% Aldrich) and 0.1 mL of tetrabutyl titanate in a teflon-lined stainless steel autoclave (50 mL). The mixture was stirred at ambient conditions for 1 min followed by the addition of 1 mL hydrochloric acid (37 wt%). After stirring for another 5 min, one piece of Ti foil substrate (0.5 cm × 0.5 cm) was placed in the teflon-liner, which was initially ultrasonically cleaned in acetone, subsequently immersed in a H_2O_2 (30 wt%, 5 mL) solution for 10 min, and finally rinsed with ethanol and deionized water. Solvent-thermal synthesis was conducted at 180 °C for 2 h in an electric oven to obtain the as-prepared TiO_2 nanorod arrays grown from Ti foil substrate. Subsequently, the TiO_2 nanorod arrays/Ti was heated to 800 °C under ammonia for 3 h with a progressive, slow heating ramp (room temperature to 300 °C, 5 °C min^{-1}; 300–700 °C, 2 °C min^{-1}; 700–800 °C, 1 °C min^{-1}). After cooled down to the room temperature, TiN NRAs grown from Ti foil substrate were finally obtained.

2.2. Fabrication of TiN NRAs based bioelectrode

HRP/Nafion/TiN NRAs was prepared as described by Lan and his co-workers with minor revision (Teng et al., 2009). 100 μL HRP (300 U mg^{-1}, Sangon, China) (5 mg mL^{-1}) was mixed with 10 μL Nafion. Then 8 μL mixtures were dropped on the TiN NRAs/Ti substrate and allowed to dry under ambient conditions overnight. The modified electrodes were rinsed with deionized water twice. Laccase/chitosan/TiN NRAs (LAC/CS/TiN NRAs) was constructed as follows: firstly, 1% chitosan (CS, from crab shells, minimum 95% deacetylation) solution was prepared by dissolving CS in 2% acetic acid solution with magnetic stirring for about 2 h. Secondly, 1 mL 1% CS was mixed thoroughly with 5 mg of laccase (93.6 U mg^{-1}, Sigma, China). Then 8 μL of the laccase/CS mixture were dropped on the TiN NRAs/Ti substrate and allowed to dry for 24 h at 4 °C. The one side surface area of both HRP/Nafion/TiN NRAs and LAC/CS/TiN NRAs electrode is 0.25 cm^2 (the other side was sealed with paraffin).These enzymatic electrodes were stored in PBS (pH 7.0) at 4 °C.

2.3. Apparatus and measurements

X-ray diffraction (XRD) patterns were recorded with a Bruker-AXS Micro-diffractometer (D8 ADVANCE) using Cu Kα radiation (λ = 1.5406 Å) from 30° to 80° at a scanning speed of 0.33° min^{-1}. Morphological information was attained from field emission scanning electron microscopy (FESEM, HITACHI S-4800, Japan). High-resolution transmission electron microscopy measurement (HRTEM) was performed using a transmission electron microscopy (JEOL 4000EX, Japan) operated at 400 keV. UV–vis absorption spectra were recorded by a UV-4100 spectrophotometer (HITACHI, Japan) with a labsphere. The baseline of UV spectrum was obtained before the immobilization of HRP on TiN NRAs electrode.

Cyclic voltammetry, linear sweep voltammetry were conducted by a CHI440a electrochemical workstation (CHI Instruments, Shanghai Chenhua Instrument Corporation, China). The as-prepared electrode was used as a working electrode. Ag/AgCl electrode and Pt foil were used as the reference electrode and counter electrode, respectively. Electrochemical impedance spectroscopy (EIS) measurement was carried out using a ZAHNER ZENNIUM electrochemical workstation with a three-electrode system by applying an AC voltage of 5 mV amplitude in the frequency range from 0.1 Hz to 100 kHz, at room temperature. The sample and buffer solutions were purged with N_2 for 30 min to remove oxygen before the experiments. Galvanostatic discharge measurements were conducted with a bio-Li–air fuel cell using a charge–discharge tester (LAND).

A preliminary lithium–air fuel cell was assembled using 1 M $LiPF_6$ in EC/DMC as the electrolyte for the Li-anode and O_2-saturated acetate buffer (pH = 4.5) with the presence of 2 mM 2,2′-azino-bis(3-ethylbenzthiazoline-6-sulphonic acid) (ABTS) as the electrolyte for the LAC/CS/TiN NRAs biocatalytic cathode. The two electrolytes were separated by a water-stable LISICON film ($Li_{1+x+y}Al_xTi_{2-x}Si_yP_{3-y}O_{12}$, provided by Ohara Inc., Japan).

3. Results and discussion

3.1. Characterization of TiN NRAs

TiN NRAs were obtained by converting TiO_2 NRAs using ammonia annealing at high temperature. During the process, the slow heating ramp was critical for successful preparation of TiN NRAs, as the fast one usually resulted in the aggregation of the nanorods (Fig. S1, Supporting Information). As depicted in Fig. 1a, the

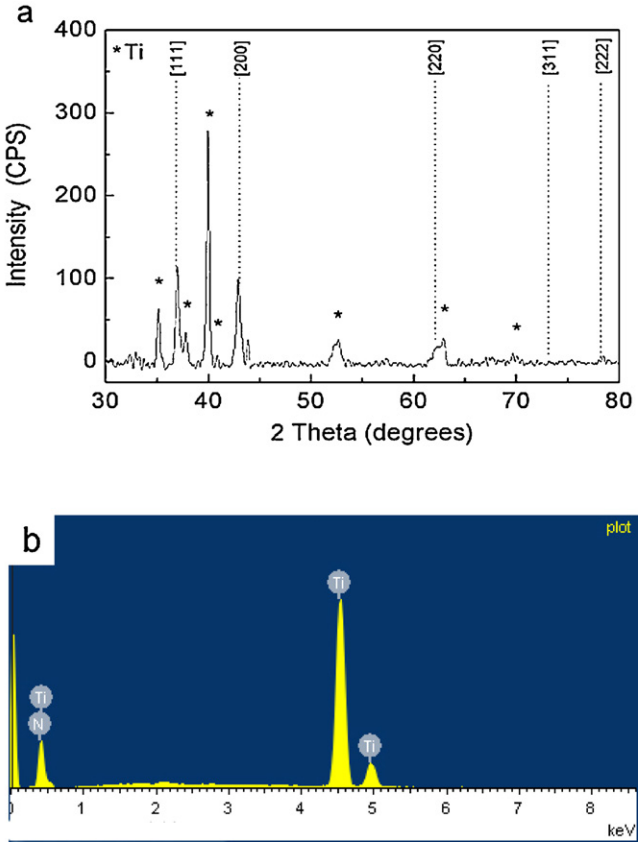

Fig. 1. X-ray diffraction pattern (a) and the electron dispersive X-ray spectrum (b) of prepared TiN nanorod arrays on the Ti foil substrate.

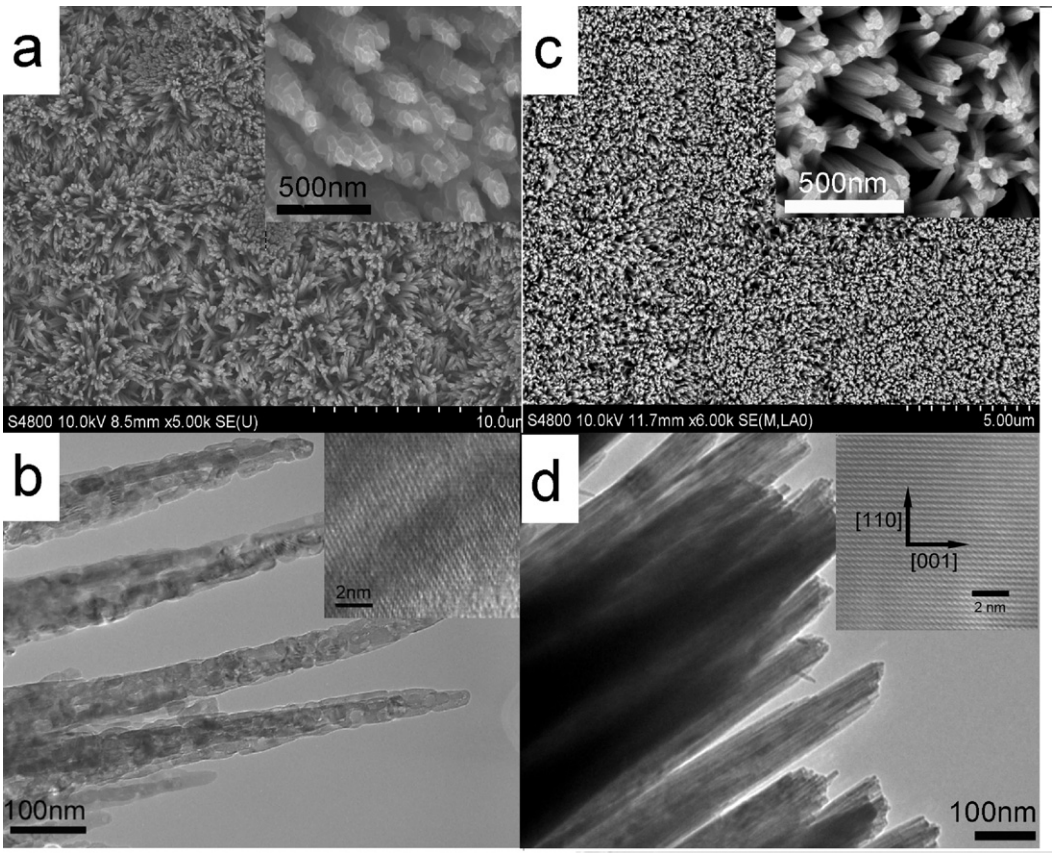

Fig. 2. FESEM and TEM images of TiN NRAs (a and b) and TiO_2 (c and d) NRAs: (a) low magnification and high magnification FESEM images (inset); (b) TEM image and HRTEM image of the TiN NRAs (inset); (c) low magnification FESEM and high magnification FESEM images (inset); (d) TEM image and HRTEM image of the TiO_2 NRAs (inset).

diffraction peaks of the nanorod arrays were indexed to the typical pattern of the cubic titanium nitride (JCPDS No. 87-0630, $a = b = c = 0.422$ nm; belonging to the space group $Fm3m$), except the peaks belonging to Ti foil substrates, which is indicative of the successful conversion of TiO_2 into TiN. Furthermore, the EDX spectrum (Fig. 1b) displayed the presence of only Ti and N, which was also in good agreement with the result of XRD.

The FESEM images of a typical TiN nanorod arrays sample at different magnifications are displayed in Fig. 2a. These images revealed that the entire surface of the Ti substrate was covered uniformly with aligned TiN nanorods. The surface morphology of the prepared TiN NRAs was analogous to that of the TiO_2 NRAs (Fig. 2c) at low magnification. However, the TiN nanorod showed a scraggly surface at high magnification (Fig. 2a, inset) due to the lattice shrinkage during the structure recrystallization. The average diameter and length of nanorods, were 45 ± 5 nm and 1.5 ± 0.2 μm, respectively. These results were further confirmed by the TEM study. In contrast to the single-crystal structure of entire TiO_2 nanorod (Fig. 2d), high resolution TEM image of TiN NRAs (Fig. 2b) indicates the polycrystalline characteristic of the materials. The lattice fringes with spacings of 0.244 and 0.211 nm were observed corresponding to the [1 1 1] and [2 0 0] planes of TiN, which confirmed that the nanorod arrays were composed of a polycrystalline cubic-structured phase.

3.2. Electrochemical catalysis of H_2O_2 and its electrochemical sensing based on TiN NRAs

H_2O_2 is not only a byproduct of several highly selective oxidation reactions catalyzed by oxidases, but also an essential mediator in food, pharmaceutical, clinical, industrial, environmental analysis (Schreier et al., 1996). Therefore the sensitive and accurate detection of H_2O_2 is of great importance to these analyses. Fig. 3a presents the cyclic voltammograms (CVs) of TiN NRAs (solid line) and TiO_2 NRAs (dotted line) in the absence and presence of H_2O_2. The reduction current increased at the TiN NRAs electrode with the addition of 1 mM H_2O_2, indicating an obviously electrochemical catalytic reduction of H_2O_2 at the electrode. As expected, the reduction current of TiN NRAs increased much more significantly than that of TiO_2 NRAs, which is attributed to the superior electrical conductivity of TiN NRAs (Zayats et al., 2008). The capability of charge transfer of the two electrodes was further investigated by AC impedance experiments (Fig. 3b). The obviously decreased semicircle of TiN NRAs suggested the lower charge transfer resistance (102.6 Ω, Supporting Information), which also indicated higher electrochemical activity of TiN NRAs (Lo et al., 2008; Zhou et al., 2009).

The CV curves in Fig. 3c shows the amperometric responses of TiN NRAs electrodes with successive additions of H_2O_2, the reduction current increased with the increasing H_2O_2 concentration correspondingly. Under a low operational potential of −0.05 V, the linear relationship between the electrocatalytic current and the concentration of H_2O_2 at TiN NRAs electrodes is observed in inset of Fig. 3c. The linear range was from 0.5 μM to 2 mM, and the LOD was 0.5 μM at S/N = 3. This linear relationship is wider than the previous results, as such carbon nanotubes/chitosan modified electrode (16.7–740 μM) (Qian and Yang, 2006), and Prussian blue modified electrode (1–400 μM) (Liu et al., 2009). The LOD was significantly lower than that of the paste electrode based on carbon nanotubes (60 μM) (Rubianes and Rivas, 2003), carbon spheres/palladium composite supported polyaniline (5.84 μM) (Kong et al., 2010), and

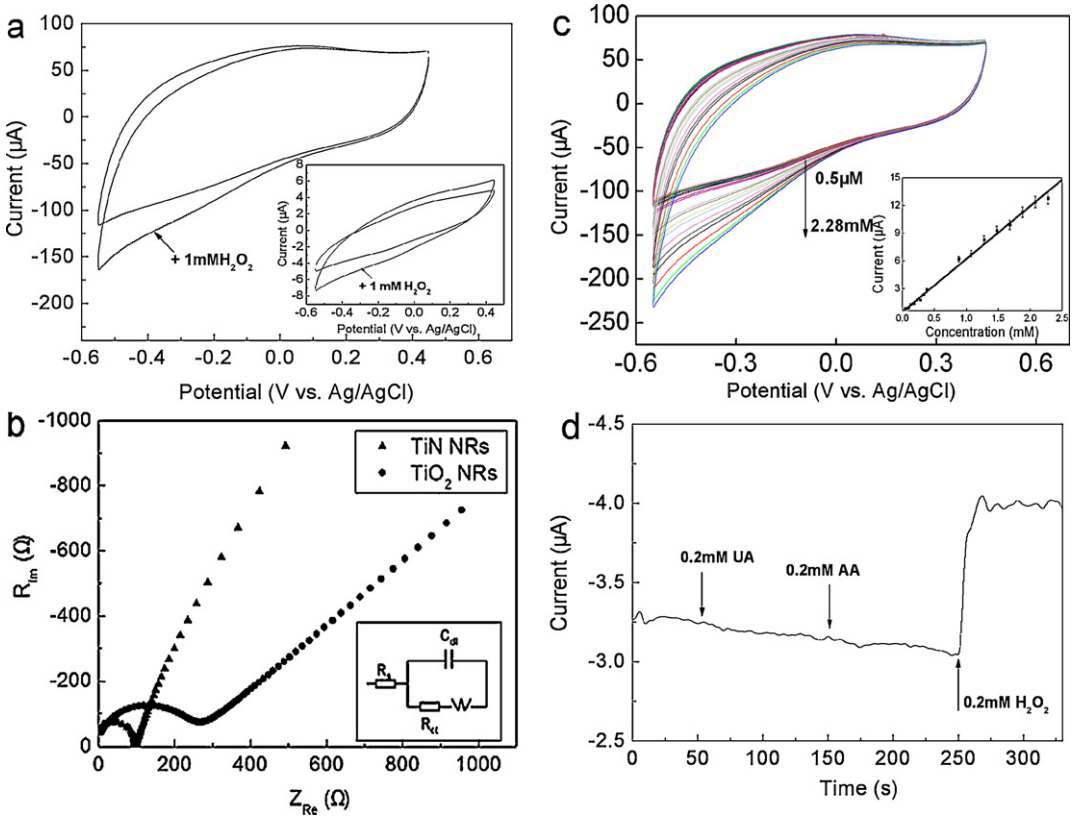

Fig. 3. (a) Cyclic voltammograms of TiN NRAs and TiO_2NRAs (inset) in the presence (pointed by arrow) and absence of 1 mM H_2O_2 in 0.2 M PBS (pH 7.0) at a scan rate of 20 mV s^{-1}. (b) Electrochemical impedance spectroscopy plots for TiN NRAs (triangle) and TiO_2 NRAs (circle) in 0.2 M PBS with open circuit voltage and amplitude of 5 mV over a frequency range from 0.1 Hz to 100 kHz. Inset is the equivalent circuit. (c) Cyclic voltammograms of TiN NRAs in 0.2 M PBS (pH 7.0) solution at a scan rate of 20 mV s^{-1} with H_2O_2 concentration ranging from 0.5 μM to 2.28 mM. Inset: plot of the electrocatalytic current versus H_2O_2 concentration for TiN NRAs in 0.2 M PBS (pH 7.0) at the operating potential of −0.05 V. (d) Amperometric response of 0.2 mM H_2O_2 in the presence of 0.2 mM AA and UA, at the TiN NRAs electrode in 0.2 M PBS (pH 7.0) at the operating potential of −0.05 V.

poly(aniline-co-p-aminophenol) based electrode (1.25 μM) (Chen et al., 2009).

In addition, with the TiN NRAs at such a low operation potential of −0.05 V, 0.2 mM uric acid (UA), ascorbic acid (AA) did not show interferences (Fig. 3d), respectively to 0.2 mM H_2O_2 detection, indicating high selectivity of TiN NRAs for H_2O_2 detection.

3.3. *Electrocatalysis of horseradish peroxidase for H_2O_2 biosensing based on TiN NRAs*

It was demonstrated that the enhanced electrochemical reactivity of TiN NRAs for H_2O_2 determination by above-discussed result, which encouraged us to further investigate the bio-electrochemical application based on TiN NRAs. In this part, HRP was chosen for fabricating TiN NRAs based enzymatic amperometric biosensor, since HRP is a commercially available representative for investigating the dynamic mechanism of the enzyme reactions (Elkaoutit et al., 2008; Teng et al., 2009).

Since the location of the UV–vis Soret absorption band of iron provides structural information about conformational change in the heme-group region, UV-vis spectrophotometer was widely used to probe the structure change for heme proteins (Theorell and Ehrenberg, 1951; Zhu et al., 2002). The UV–vis spectra of TiN NRAs electrode after the immobilization of HRP with Nafion (subtracting the spectrum of TiN NRAs as baseline) is shown in Fig. 4. A characteristic absorption band centered at of 408 nm indicated the immobilization of HRP on TiN NRAs (Theorell and Ehrenberg, 1951; Zhu et al., 2002). The Soret band of HRP entrapped in the HRP/Nafion/TiN NRAs electrode was only a little shift from that of

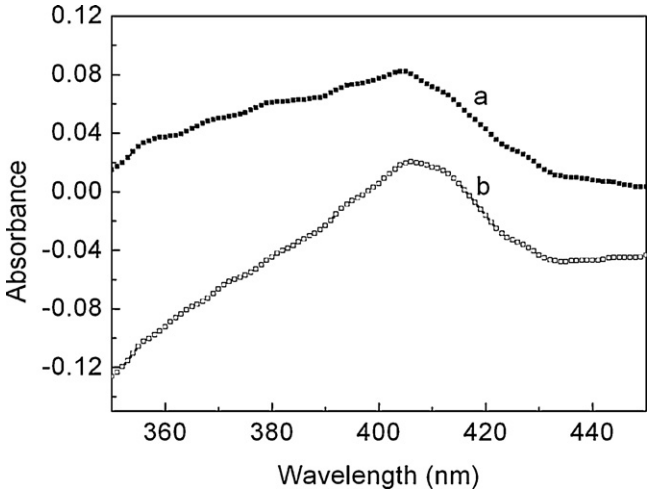

Fig. 4. UV–vis spectrum of the immobilized HRP on TiN NRAs electrode (a) and UV–vis spectrum of the natural HRP film deposited on quartz plate (b).

the natural HRP film deposited on quartz plate, which was also agreed with previous reports (Lu et al., 2010a,b; Teng et al., 2009; Xiao et al., 2009). This result indicated that HRP entrapped in the composite electrode had a secondary structure similar to native state of HRP, which suggested that TiN NRAs could deliver good biocompatibility for HRP.

The typical electrochemical behavior of HRP/Nafion/TiN NRAs electrode in the PBS solution containing 1.0 mM methylene blue

(MB) at different scan rates is depicted in Fig. 5a. MB was added and used as an electron mediator to further improve the sensitivity of the proposed H_2O_2 biosensor (Kafi et al., 2008). A couple of well-characterized reduction/oxidation peaks were observed at −0.22 V and −0.17 V respectively, which was due to presence of MB (Yan et al., 2005; Yan et al., 2009; Zhang et al., 2010). Moreover, the peak currents are proportional to the square roots of the scan rates (inset in Fig. 5a), which is a typical semi-infinite linear diffusion-controlled electrochemical behavior feature of the redox process (Lu et al., 2010a,b).

In order to test the activity of HRP immobilized on TiN NRAs, its response to the reduction of H_2O_2 was examined. As shown in Fig. 5b, the reduction peak of MB increased with an increasing H_2O_2 concentration. The reaction mechanism of the biosensor can be summarized as follows (Chen et al., 2006):

$$\mathrm{HRP\ (red)} + \mathrm{H_2O_2} \rightarrow \mathrm{HRP(ox)} + \mathrm{H_2O} \quad (1)$$

$$\mathrm{HRP(ox)} + \mathrm{MB(red)} \rightarrow \mathrm{HRP(red)} + \mathrm{MB(ox)} \quad (2)$$

$$\mathrm{MB(ox)} + \mathrm{e^-} \rightarrow \mathrm{MB(red)} \quad (3)$$

Firstly, hydrogen peroxide in the electrolyte is reduced by the HRP (red), forming HRP (ox). Secondly, HRP (ox) can be regenerated with the help of the mediator MB, while the MB (red) is oxidized in the enzymatic reaction. Finally, the MB (ox) is electrochemically reduced on the electrode surface, resulting in the increase of reduction current.

The calibration curve of H_2O_2 biosensing is shown in the Fig. 5c. Although the linear calibration range of the analyte was only up to 2 μM, this HRP/Nafion/TiN NRAs electrode was very sensitive to the concentration of H_2O_2. The LOD can reach 0.05 μM, which was lower than that of the previous reports (Kafi et al., 2008; Liu et al., 2008; Lu et al., 2010a,b; Xiang et al., 2009; Xiao et al., 2009). The long-term stability of this biosensor was also investigated. It retained 95% of its initial current response after 30 days.

3.4. TiN NRAs based enzymatic air-electrode for Li –air fuel cell

Since the HRP/Nafion/TiN NRAs electrode exhibits promising enzymatic activity, it is reasonable to expect that TiN NRAs can be promising for enzyme-derived electrochemical energy conversion. Therefore, we constructed a novel bioelectrochemical energy conversion system based on enzyme/TiN NRAs electrode. Laccase, as an enzyme specific for catalyzing a four-electron reduction of O_2, has been immobilized on TiN NRAs as the cathode biocatalyst in Li–air fuel cell. The structure of the bio-Li–air fuel cell is close to that of the H_2O_2 fuel cell, which is generally composed by anode (a noble metal based catalyst oxidizes the H_2-fuel), proton exchanged membrane, and cathode (noble metal reduction O_2). As shown in Fig. 6a, we proposed to use the LAC/CS/TiN NRAs enzymatic electrode working in aqueous solution (in the presence of 2 mM ABTS) as the oxygen biocatalytic cathode, which replaced the noble metal based cathode materials, Li metal working in organic electrolyte as the solid-state Li-fuel anode, and ceramic LISICON (lithium superionic conductor) film as a separator to fabricate the bio-Li–air fuel cell. The LISICON film is stable in both aqueous and organic electrolyte, which consequently separates oxygen biocatalytic cathode (in aqueous electrolyte) and metallic Li-anode (in organic electrolyte). The Li-anode is converted into Li-ions and these Li-ions in organic electrolyte solution diffuse to aqueous solution across the ceramic LISICON film. The catalysis mechanism of cathode reaction can be summarized as follows (Palmore and Kim, 1999; Quan et al., 2004):

$$\mathrm{Laccase(ox)} + \mathrm{ABTS} \rightarrow \mathrm{Laccase(red)} + \mathrm{ABTS^{\bullet +}} \quad (4)$$

$$\mathrm{Laccase(red)} + \mathrm{O_2} + 4\mathrm{H^+} + 4\mathrm{e^-} \rightarrow \mathrm{Laccase(ox)} + 2\mathrm{H_2O} \quad (5)$$

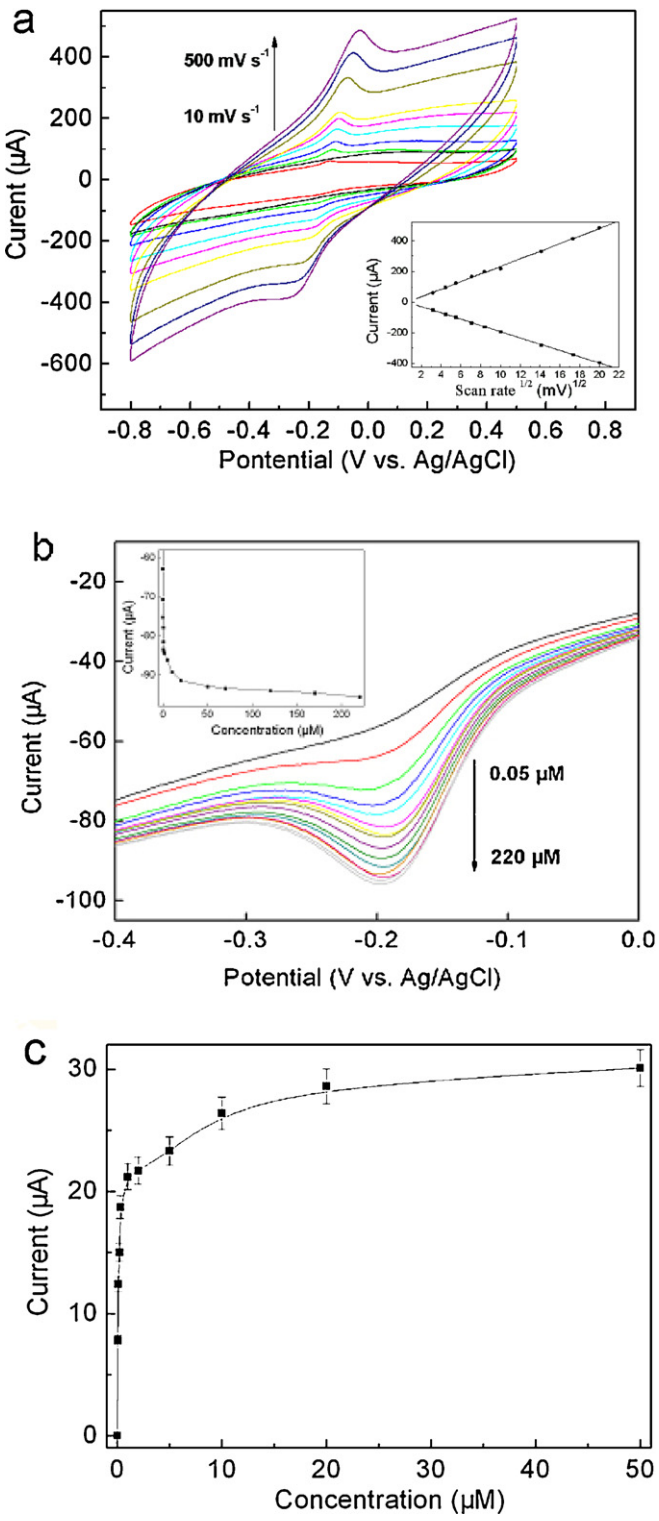

Fig. 5. (a) Cyclic voltammogram curves of the HRP/TiN NRAs electrode in 0.2 M PBS (pH 7.0) containing 1.0 mM methylene blue at different scan rates (inner to outer): 10 mV s^{-1}, 20 mV s^{-1}, 30 mV s^{-1}, 50 mV s^{-1}, 70 mV s^{-1}, 100 mV s^{-1}, 200 mV s^{-1}, 300 mV s^{-1}, 500 mV s^{-1}. Inset: dependence of the redox peak currents on the square root of scan rates. (b) Linear sweep voltammograms of HRP/TiN NRAs electrode in 0.2 M PBS (pH 7.0) solution at a scan rate of 20 mV s^{-1} with H_2O_2 concentration range from 0.05 μM to 228 μM. Inset: plot of the peak of reduction current versus H_2O_2 concentration for HRP/TiN NRAs in 0.2 M PBS (pH 7.0) at the operating potential of −0.22 V. (c) Plot of the electrocatalytic current versus H_2O_2 concentration for HRP/TiN NRAs in 0.2 M PBS (pH 7.0) at the operating potential of −0.22 V.

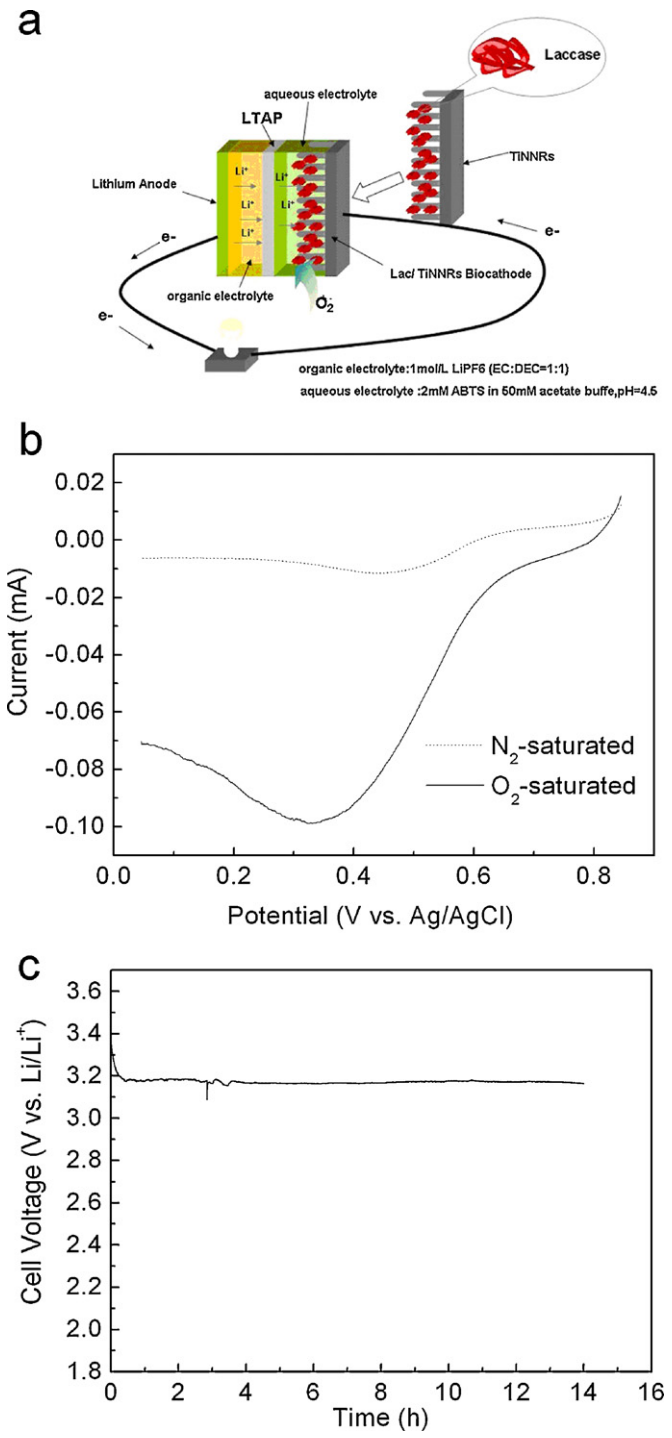

Fig. 6. (a) A schematic illustration for the structure of bio-Li–air fuel cell based on LAC/TiN NRAs biocatalyst cathode. (b) Polarization curves of LAC/TiN NRAs electrode in N_2-saturated (dashed) or O_2-saturated (solid line) 50 mM acetate buffer (pH 4.5) with the presence of 2 mM ABTS at a scan rate of 20 mV s^{-1}. (c) Discharge curve of the prepared Bio-Li–air fuel cell.

The anode and overall reaction of the cell can be respectively expressed as:

$$Li \rightarrow Li^+ + e^- \quad (6)$$

$$4Li + 2O_2 + 4H^+ \leftrightarrow 4Li^+ + 2H_2O \quad (7)$$

ABTS, a general substrate of laccase, functions as an electron mediator in electrochemical study. As shown in Fig. 6b, the reduction peak of ABTS with formal potential of 0.48 V was observed in 50 mM N_2-saturated acetate buffer (pH 4.5). In O_2-saturated solution, the reduction peak current significantly increased due to the reduction of the catalytically oxidized $ABTS^{\bullet+}$, which represented a typically electrocatalytic reduction of oxygen by laccase (Liu et al., 2006; Rowi'nski et al., 2004).

The discharge curve of the prepared bio-Li–air fuel cell is displayed in Fig. 6c with a test current of 0.25 mA cm^{-2}, which open circuit voltage (OCV) was about 3.69 V (versus Li/Li^+). At the beginning of discharge, the operating voltage of the prepared lithium–air fuel cell reduced sharply. Then, the operating voltage kept at about 3.19 V on the consequent discharge process. During the prolonged discharge process, the cathodic reaction was attributed to bio-electrocatalytic O_2 reduction reaction. The rapid decrease in operating voltage at the beginning of discharge can be attributed to the electrode polarization. However, the 3.19 V operating voltage is still higher than that of Li–air batteries cell with organic electrolytes (Débart et al., 2008; Wang and Zhou, 2010; Xiao et al., 2010).

The above preliminary results demonstrate the feasibility of a lithium–air fuel cell with laccase integrated on TiN NRAs as a biocatalyst for O_2 electrochemical reduction. Although there are some issues to be addressed in this system, such as the prolonged performance of biocatalyst, this part of study here suggests that TiN NRAs with unique 1D array structure can act as a promising biocompatible nanostructured electrode for the integration of biocatalyst in electrochemical energy conversion systems.

4. Conclusions

In summary, the application of TiN NRAs as a biocompatible nanostructured electrode in bio-electrochemical system has been proposed. Because of the unique nanostructure and excellent electronic conductivity, the TiN NRAs exhibited superior electrocatalytic activity towards H_2O_2. The electrochemical sensing of H_2O_2 is showed to deliver a wide linear range of 0.5 μM–2 mM, low LOD (0.5 μM), and high selectivity with the interferences of UA and AA. Additionally, on the basis of excellent biocompatibility of TiN, TiN NRAs based HRP biosensor displayed enhanced analytical sensitivity of H_2O_2 with a LOD of 0.05 μM. These results further inspired the exploration of LAC/CS/TiN NRAs biocatalytic cathode in a novel bio-Li–air fuel cell system, which offers an alternative to noble metal catalyst. As shown in the above discussion, TiN NRs can be extremely attractive as a nanostructured electrode for a wide range of bio-electrochemical applications, ranging from bio-electrochemical sensing to bio-electrochemical energy conversion systems.

Acknowledgements

We appreciate the support of "100 Talents" program of the Chinese Academy of Sciences, National Program on Key Basic Research Project of China (973 Program) (No. MOST2011CB935700), Shandong Province Fund for Distinguished Young Scientist (BS2009NJ013) and National Natural Science Foundation of China (Grant Nos. 20971077, 20901044, 20802039 and 20902052).

Appendix A. Supplementary data

Supplementary data associated with this article can be found, in the online version, at doi:10.1016/j.bios.2011.03.040.

References

Chen, C.X., Sun, C., Gao, Y.H., 2009. Electrochem. Commun. 11, 450–453.
Chen, S., Yuan, R., Chai, Y., Xu, L., Wang, N., Li, X., Zhang, L., 2006. Electroanalysis 18, 471–477.

Choi, D., Kumta, P.N., 2006. J. Electrochem. Soc. 153, A2298.
Débart, A., Paterson, A.J., Bao, J., Bruce, P.G., 2008. Angew. Chem. Int. Ed. 47, 452–4524.
Deng, L., Wang, F., Chen, H., Shang, L., Wang, L., Wang, T., Dong, S., 2008. Biosens. Bioelectron. 24, 329–333.
Drygas, M., Czosnek, C., Paine, R.T., Janik, J.F., 2006. Chem. Mater. 18, 3122.
Elkaoutit, M., Naranjo-Rodriguez, I., Dominguez, M., Hernandez-Artiga, M.P., Bellida-Milla, D., de Cisneros, J., 2008. Electrochim. Acta 53, 7131–7137.
Feng, X., Shankar, K., Varghese, O.K., Paulose, M., Latempa, T.J., Grimes, C.A., 2008. Nano Lett. 8, 3781.
Fischer, A., Makowski, P., Muller, J.O., Antonietti, M., Thomas, A., Goettmann, F., 2008. ChemSusChem 1, 444.
Hyde, G.K., McCullen, S.D., Jeon, S., Stewart, S.M., Jeon, H., Loboa, E.G., Parsons, G.N., 2009. Biomed. Mater. 4, 1–10.
Kafi, A.K.M., Wu, G., Chen, A., 2008. Biosens. Bioelectron. 24, 566–571.
Kaskel, S., Schlichte, K., Kratzke, T., 2004. J. Mol. Catal. A: Chem. 208, 291.
Kirchner, C.N., Hallmeier, K.H., Szargan, R., Raschke, T., Radehaus, C., Wittstock, G., 2007. Electroanalysis 19, 1023.
Katz, E., Lioubashevski, O., Willner, I., 2005. J. Am. Chem. Soc. 127, 3979.
Kong, L., Lu, X., Bian, X., Zhang, W., Wang, C., 2010. Langmuir 26, 5985–5990.
Liu, Y., Chu, Z., Jin, W., 2009. Electrochem. Commun. 11, 484–487.
Liu, Y., Lei, J., Ju, H., 2008. Talanta 74, 965–970.
Liu, Y., Qu, X., Guo, H., Chen, H., Liu, B., Dong, S., 2006. Biosens. Bioelectron. 21, 2195–2201.
Lo, P.-H., Kumar, S.A., Chen, S.-M., 2008. Colloids Surf. B: Biointerfaces 66, 266–273.
Lu, L., Zhang, Li., Zhang, X., Wu, Z., Huan, S., Shen, G., Yu, R., 2010a. Electroanalysis 22, 471–477.
Lu, Y.-C., Xu, Z., Gasteiger, H.A., Chen, S., Hamad-Schifferli, K., Shao-Horn, Y., 2010b. J. Am. Chem. Soc. 132, 12170–12171.
Muhammed Musthafa, O.T., Sampath, S., 2008. Chem. Commun. 1, 67.
Njagi, J., Chernov, M.M., Leiter, J.C., Andreescu, S., 2010. Anal. Chem. 82, 989–996.
Noh, H.-B., Won, M.-S., Hwang, J., Kwon, N.-K., Shin, S.C., Shim, Y.-B., 2010. Biosens. Bioelectron. 25, 1735–1741.
Palmore, G.T.R., Kim, H.H., 1999. J. Electroanal. Chem. 464, 110–117.
Qian, L., Yang, X., 2006. Talanta 68, 721–727.
Qiu, Y., Gao, L., 2005. J. Phys. Chem. B 109, 19732.
Quan, D., Kim, Y., Shin, W., 2004. J. Electroanal. Chem. 561, 181–189.
Ramanavicius, A., Ramanaviciene, A., 2009. Fuel Cells 9, 25–36.
Rowi'nski, P., Bilewicz, R., St'eb'e, M.J., Rogalska, E., 2004. Anal. Chem. 76, 283–291.
Rubianes, M.D., Rivas, G.A., 2003. Electrochem. Commun. 5, 689–694.
Schreier, T.M., Rach, J.J., Howe, G.E., 1996. Aquaculture 140, 323–331.
Serro, A.P., Completo, C., Colaço, R., dos Santos, F., Lobato da Silva, C., Cabral, J.M.S., Araújo, H., Pires, E., Saramago, B., 2009. Surf. Coat. Technol. 203, 3701–3707.
Snyder, M.Q., Trebukhova, S.A., Ravdel, B., Wheeler, M.C., DiCarlo, J., Tripp, C.P., DeSisto, W.J., 2007. J. Power Sources 165, 379.
Swensen, J.S., Xiao, Y., Ferguson, B.S., Lubin, A.A., Lai, R.Y., Heeger, A.J., Plaxco, K.W., Soh, H.T., 2009. J. Am. Chem. Soc. 131, 4262–4266.
Tasca, F., Gorton, L., Harreither, W., Haltrich, D., Ludwig, R., Noll, G., 2008. J. Phys. Chem. C112, 9956–9961.
Teng, Y.J., Zuo, S.H., Lan, M.B., 2009. Biosens. Bioelectron. 24, 1353–1357.
Theorell, H., Ehrenberg, A., 1951. Acta Chem. Scand. 5, 823–848.
Wang, R., Ruan, C., Kanayeva, D., Lassiter, K., Li, Y., 2008. Nano Lett. 8, 2625–2631.
Wang, Y., Yuan, H., Lu, X., Zhou, Z., Xiao, D., 2006. Electroanalysis 18, 1493.
Wang, Y., Zhou, H., 2010. J. Power Sources 195, 358–361.
Xiang, C.L., Zou, Y.J., Sun, L.X., Xu, F., 2009. Sens. Actuators B 136, 158–162.
Xiao, J., Xu, W., Wang, D., Zhang, J.-G., 2010. J. Electrochem. Soc. 157, A294–297.
Xiao, P., Garcia, B.B., Guo, Q., Liu, D., Cao, G., 2007. Electrochem. Commun. 9, 2441–2447.
Xiao, X.L., Luan, Q.F., Yao, X., Zhou, K.B., 2009. Biosens. Bioelectron. 24, 2447–2451.
Yan, Y., Zhang, M., Gong, K., Su, L., Guo, Z., Mao, L., 2005. Chem. Mater. 17, 3457–3463.
Yan, Y.M., Baravik, I., Tel-Vered, R., Willner, I., 2009. Adv. Mater. 21, 1–5.
Yang, K., She, G., Wang, H., Ou, X., Zhang, X.-H., Lee, C.-S., Lee, S.-T., 2009. J. Phys. Chem. C 113, 20169–20172.
Yao, W., Makowski, P., Giordano, C., Goettmann, F., 2009. Chem. Eur. J. 15, 11999.
Zayats, M., Willner, B., Willner, I., 2008. Electroanalysis 20, 583–601.
Zelada-Guillén, G.A., Riu, J., Düzgün, A., Rius, F.X., 2009. Angew. Chem. Int. Ed. 48, 7334–7337.
Zhang, Y., Liu, L., Xi, F., Wu, T., Lin, X., 2010. Electroanalysis 22, 277–285.
Zhang, Y., Xiao, P., Zhou, X., Liu, D., Garcia, B.B., Cao, G., 2009. J. Mater. Chem. 19, 948–953.
Zhou, M., Du, Y., Chen, C., Li, B., Wen, D., Dong, S., Wang, E., 2010. J. Am. Chem. Soc. 132, 2172–2174.
Zhou, M., Shang, L., Li, B., Huang, L., Dong, S., 2008. Biosens. Bioelectron. 24, 442–447.
Zhou, M., Zhai, Y., Dong, S., 2009. Anal. Chem. 81, 5603–5613.
Zhu, Y.C., Cheng, G.J., Dong, S.J., 2002. Biophys. Chem. 97, 129–138.